

Comparison and calibration of MP2RAGE quantitative T1 values to multi-TI inversion recovery T1 values

Adam M. Saunders,^{a*} Michael E. Kim,^b Chenyu Gao,^a Lucas W. Remedios,^b Aravind R. Krishnan,^a Kurt G. Schilling,^{c,d} Kristin P. O'Grady,^{c,e} Seth A. Smith,^{c,e} Bennett A. Landman^{a-e}

^aDepartment of Electrical and Computer Engineering, Vanderbilt University, Nashville, TN, United States

^bDepartment of Computer Science, Vanderbilt University, Nashville, TN, United States

^cVanderbilt University Institute of Imaging Science, Vanderbilt University Medical Center, Nashville, TN, United States

^dDepartment of Radiology and Radiological Sciences, Vanderbilt University Medical Center, Nashville, TN, United States

^eDepartment of Biomedical Engineering, Vanderbilt University, Nashville, TN, United States

*adam.m.saunders@vanderbilt.edu

Abstract

While typical qualitative T1-weighted magnetic resonance images reflect scanner and protocol differences, quantitative T1 mapping aims to measure T1 independent of these effects. Changes in T1 in the brain reflect chemical and physical changes in brain tissue, such as the demyelination of axons in multiple sclerosis. Magnetization-prepared two rapid acquisition gradient echo (MP2RAGE) is an acquisition protocol that allows for efficient T1 mapping with a much lower scan time per slice compared to multi-TI inversion recovery (IR) protocols. We collect and register B1-corrected MP2RAGE acquisitions with an additional inversion time (MP3RAGE) alongside multi-TI selective inversion recovery acquisitions for four subjects and find a tissue-dependent bias between the derived T1 values. We train a patch-based ResNet-18 to calibrate the MP3RAGE T1 values to the multi-TI IR T1 values, incorporating the standard deviation of T1 calculated from a Monte Carlo simulation as an additional channel. Across four folds, the error between the MP2RAGE and T1 maps varies substantially (RMSE in white matter: 0.30 ± 0.01 seconds, subcortical gray matter: 0.26 ± 0.02 seconds, cortical gray matter: 0.36 ± 0.02 seconds). Our network reduces the RMSE significantly (RMSE in white matter: 0.11 ± 0.02 seconds, subcortical gray matter: 0.10 ± 0.02 seconds, cortical gray matter: 0.17 ± 0.03 seconds). Adding the standard deviation channel does not substantially change the RMSE. Using limited paired training data from both sequences, we can reduce the error between quantitative imaging methods and calibrate to one of the protocols with a neural network.

Keywords: quantitative imaging, T1 mapping, MP2RAGE, multi-TI inversion recovery, calibration

1. Introduction

Typical structural magnetic resonance imaging (MRI) produces a qualitative image where the voxel values are weighted by the magnetic resonance tissue relaxation parameters. Anatomical information, scanner differences and acquisition protocol differences affect the voxel values in structural MRI [1]. In contrast, quantitative MRI aims to produce maps of specific parameters, such as T1, T2, and proton density, with voxels representing the quantitative value instead of arbitrary units, designed to provide a reproducible, standardized metric [1]. Quantitative MRI can provide the ability to infer histological information noninvasively [1,2].

Quantitative imaging of the longitudinal relaxation parameter T1, often referred to as T1 mapping, has found applications in studying heart diseases [3] as well as neurodegenerative diseases [1]. Changes in T1 values represent changes in the physical and chemical properties of brain tissue and can serve as a biomarker for diseases. For example, while structural MRI can be used to identify tissue lesions in multiple sclerosis, it does not convey the chemical differences between lesions. T1 mapping, however, can measure differences in lesion types that correlate with disease progression [4].

There are several methods for quantitative T1 mapping. A standard family of methods are inversion recovery methods that sample the signal recovery curve at multiple points after an inversion pulse, like inversion recovery spin echo (IR-SE), although acquisition times are extremely long [5]. An alternative with a shorter acquisition time is echo planar imaging (IR-EPI) [6]. IR-EPI can suffer from spatial distortions, but Sanchez-Panchuelo et al. have proposed modifications to reduce the distortions and efficiently acquire multi-slice images [7]. Selective inversion recovery (SIR) is another multi-TI inversion recovery method that can produce quantitative T1 maps in addition to other metrics that quantify the magnetization transfer effect, with applications for studying multiple sclerosis [8,9].

An alternative to multi-TI IR T1 mapping methods with many samples along the signal recovery curve, magnetization prepared two rapid acquisition gradient echoes (MP2RAGE) allows for high-resolution and efficient quantitative T1 mapping with a much shorter acquisition time than multi-TI IR methods [10]. Quantitative T1 mapping from an MP2RAGE image involves obtaining two gradient echo readouts (GREs) and combining them to form a T1-weighted image. This T1-weighted image is independent of effects from T2* and the static magnetic field B_0 , though there are still higher-order effects from the radiofrequency field, referred to as B_1^+ . B_1^+ inhomogeneities also affect multi-TI IR acquisitions. While we can optimize the acquisition parameters for MP2RAGE to minimize effects from B_1^+ , there still may be effects from B_1^+ in the image and corresponding quantitative T1 map, and quantitative T1 mapping is sensitive to the values of B_1^+ and acquisition parameters (see supplementary figure). Eggenchwiler et al. have proposed modifications to MP2RAGE to account for inhomogeneities in B_1^+ , where a second acquisition with a similar sequence called Sa2RAGE can provide iterative estimates for T1 and B_1^+ together [11]. Quantitative T1 mapping with MP2RAGE at 7T shows high reproducibility between sites [12].

Due to the long repetition time $MP2RAGE_{TR}$ between inversion pulses, modifications to the MP2RAGE sequence can allow for collecting multiple echoes beyond the single echo collected as the second GRE in a typical MP2RAGE acquisition. Multi-echo MP2RAGE can be used to generate simultaneous quantitative mappings of T1, T2*, and quantitative susceptibility mapping [13–15]. The MPnRAGE sequence is another modification that uses a sliding window to effectively collect n images with different T1 weighting contrasts [16]. MP3RAGE collects a third GRE with a high flip angle to generate T1 maps and B_1^+ maps simultaneously with analytical solutions for T1 and B_1^+ [17]. Another method also referred to as MP3RAGE uses the third GRE to simultaneously solve for T1 and inversion pulse efficiency [18].

Marques et al. have validated quantitative T1 mapping with MP2RAGE in phantoms and in vivo with comparisons to values found in the literature [10]. Gochberg and Gore have validated quantitative T1 mapping with SIR in phantoms and in vivo with animals [19], while Bagnato et al. and Cronin et al. have studied SIR T1 maps in vivo with human brains [8,20].

Previous studies have compared co-registered quantitative T1 values from MP2RAGE to several different multi-TI IR protocols [5,7,21]. Rioux et al. found that there are significant differences between MP2RAGE quantitative T1 values and IR-FSE quantitative T1 values, potentially because a biexponential fitting for IR-FSE models the inversion recovery well to account for magnetization transfer effects, but MP2RAGE uses a monoexponential model [21]. With only two to three GREs for MP2RAGE and MP3RAGE, we are limited in the number of samples we can use to fit MP2RAGE inversion recovery to a biexponential model. The longer inversion times for MP2RAGE can mitigate this effect but do not remove it completely [21].

Here, we aim to not only compare quantitative T1 values from MP2RAGE and multi-TI IR but also calibrate the MP2RAGE T1 values to the multi-TI IR T1 values using a deep learning model. Calibration between the two methods would allow us to collect MP2RAGE scans with low scan times per slice and calibrate the T1 values to IR T1 values, which has a much higher scan time per slice. Additionally, we use a maximum a posteriori (MAP) approach to MP2RAGE quantitative T1 mapping that allows for T1 estimation from MP2RAGE and MP3RAGE acquisitions and for the additional estimation of the standard deviation of T1 as an uncertainty estimate.

2. Methods

To compare MP2RAGE T1 maps with multi-TI IR T1 maps, we obtained data from four subjects on a 7T Philips Achieva scanner. We obtained informed consent after explaining the procedure under a protocol approved by the local institutional review board. We collected a T1-weighted magnetization-prepared rapid acquisition gradient echo (MPRAGE) acquisition, a multi-TI IR acquisition, an MP2RAGE acquisition with an additional GRE (also known as an MP3RAGE acquisition), as well as a dual-TR actual flip angle acquisition for B1 correction of the MP2RAGE/MP3RAGE and multi-TI IR T1 maps.

For comparing the errors in each tissue type, we used U-shaped medical image segmentation model with nested transformers (UNesT) to segment the image [22]. We combine the labels

using a 12-level hierarchical model whose labels were selected by a neuroimaging expert [23]. We used the level with 8 clusters and analyzed clusters 3 (subcortical gray matter, SGM), 4 (cortical gray matter, CGM), and 7 (cerebral white matter, WM). Cluster 4 also included the amygdala and hippocampus, but these structures were not present in the mid-brain slices for which we collected multi-TI IR images. We eroded the CGM cluster mask with a cube with sides of length 3 voxels to mitigate partial volume effects from the cerebrospinal fluid (CSF). The other clusters were either background, CSF in the ventricles, or labels that were not present within the slices we analyzed. Next, we used the MPRAGE images to create skull-stripped masks using SynthStrip [24]. To compare the images within a common spatial framework, we registered all images to the multi-TI IR image space using a rigid registration from the ANTs registration toolkit (version 2.4.4) [25]. For registering the MP3RAGE images to multi-TI IR image space, we used a robust T1-weighted image to suppress noise, where the addition of a constant value β to the MP2RAGE signal equation can suppress noise. Here, we used a constant β value of 0.25 times the mean sum of the squared magnitudes of the GREs [26].

The multi-TI IR T1 maps were created using a voxelwise nonlinear least squares fit. Similar to the acquisition protocol described in [8], the multi-TI IR acquisition was SIR, consisting of 14 samples along the inversion recovery curve at inversion times $t_i = 6$ ms, 10 ms, 16 ms, 26 ms, 43 ms, 68 ms, 110 ms, 178 ms, 288 ms, 468 ms, 760 ms, 1230 ms, 2000 ms, and 8000 ms with a constant pre-delay time of $t_d = 2.5$ ms. We acquired these images for five axial slices with 2 mm thickness in each patient, and the scan time was approximately 7 minutes. We fit the T1 maps as in [27], assuming the relaxation rates of a two-pool model with free water and macromolecular protons are equal, $R_{1f} \approx R_{1m}$. For B1 correction of the multi-TI IR images, we simulated the inversion pulse to find the inversion pulse coefficient S_m over a range of B_1^+ values [27]. We fit the data to the biexponential SIR model using a nonlinear least squares fitting algorithm. We use the reciprocal of the longitudinal relaxation rate of free water as our value for T1; that is, $T_1 = 1/R_{1f}$.

For greater flexibility in T1 mapping while maintaining the same $MP2RAGE_{TR}$, we acquired three GREs for an MP3RAGE acquisition. The acquisition consisted of a typical MP2RAGE sequence modified by the addition of a third GRE. The acquisition parameters were inversion times $TI_1 = 1010$ ms, $TI_2 = 3683$ ms, $TI_3 = 6355$ ms, a repetition time between excitation pulses of $TR = 6$ ms, and a repetition time between inversion pulses of $MP2RAGE_{TR} = 8.25$ s. Each GRE block used 225 excitation pulses, flip angles of 4° , and an inversion pulse efficiency of 0.84. The inversion pulse efficiency was calculated from a simulation similar to the one described in Marques et al., though we found that the quantitative T1 values were largely insensitive to this value [10]. The scan time was approximately 9 minutes for 512 axial slices of 0.43 mm thickness. From the MP3RAGE acquisition, we can use the first two GREs to form a typical MP2RAGE signal. To estimate MP2RAGE T1 maps, we follow the original point estimate method from Marques et al. as a baseline using the first two GREs [10]. To summarize, the method involves acquiring two complex-valued GREs at inversion times TI_1 and TI_2 . The two GREs form the MP2RAGE signal $S_{1,2}$ as

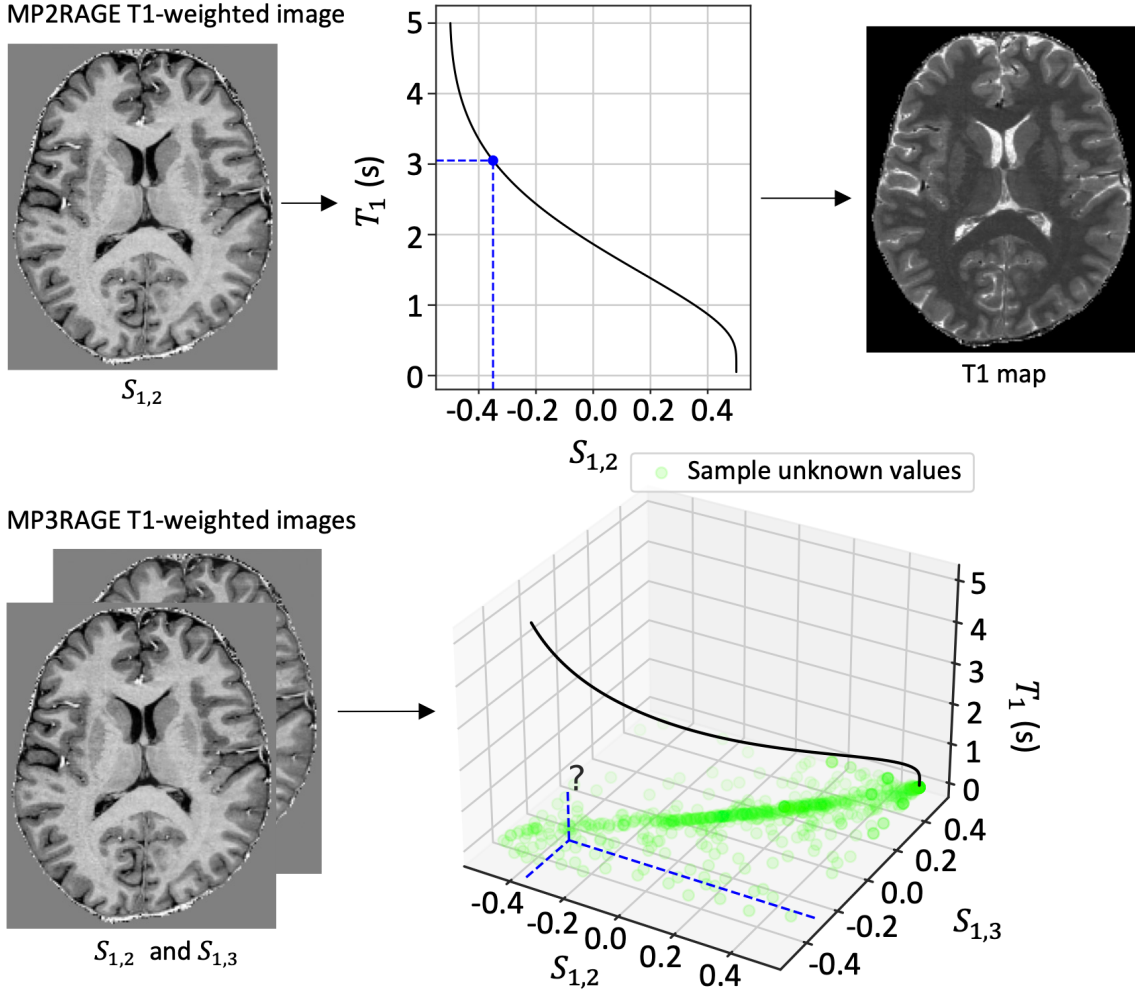


Fig. 1. Quantitative T1 mapping with MP2RAGE consists of creating a T1-weighted MP2RAGE image $S_{1,2}$ and then using the MP2RAGE signal equation to find corresponding values of T1. However, this method provides no measures of uncertainty and does not extend to MP3RAGE, where T1 values are not defined for all values of the noisy acquired MP3RAGE T1-weighted images $S_{1,2}$ and $S_{1,3}$.

$$S_{1,2} = \text{Re} \left(\frac{GRE_{T1_1}^* GRE_{T1_2}}{|GRE_{T1_1}|^2 + |GRE_{T1_2}|^2} \right), \quad (1)$$

where $*$ indicates the complex conjugate. From the acquisition parameters and the MP2RAGE signal equation [10], we can create a lookup table and estimate what the signal $S_{1,2}$ should be given a set of T1 values. We estimate T1 for the acquired signal by finding the corresponding T1 value for a given MP2RAGE signal value at each voxel.

While the MP2RAGE sequence aims to remove inhomogeneities due to the B_1^+ field by optimizing the sequence parameters [10], there are still B_1^+ biases present in the images. We must

correct these biases to accurately compare MP2RAGE T1 maps with inversion recovery T1 maps [28]. Eggenschwiler et al. and Marques et al. used B_1^+ maps generated from saturation-prepared two rapid acquisition gradient echo (Sa2RAGE) in tandem with MP2RAGE images to correct for these biases [11,29]. For B1 correction of the MP2RAGE T1 maps, we use a B1 map calculated online from the scanner from the dual-TR actual flip angle acquisition [30]. We multiply the B1 correction factor for each voxel by the nominal MP2RAGE flip angles when estimating the lookup table for the T1 maps. The derivation of the MP2RAGE signal equations by Marques et al. takes into account the efficiency for the initial inversion pulse, but there are still higher order effects of B_1^+ inhomogeneities in the radiofrequency flip angles in the GRE block. For the MP3RAGE acquisition, we could choose to treat the inversion pulse efficiency as a free parameter and fit it from the data. Because we found that the quantitative T1 values were largely insensitive to the inversion pulse efficiency, we chose to fix this value and use a separate acquisition to find the B_1^+ correction factor a priori.

The third GRE in our MP3RAGE acquisition allows us to form two T1-weighted images from pairs of the GREs, $S_{1,2}$ and $S_{1,3}$. When extending from a single T1-weighted MP2RAGE image $S_{1,2}$ to MP3RAGE images $S_{1,2}$ and $S_{1,3}$, generating a T1 map is not straightforward. Since the GRE acquisition process contains noise, we have many values in our acquired images that fall outside of the defined T1 values (Fig. 1). Previous studies have taken advantage of the long $MP2RAGE_{TR}$ to collect a third GRE but estimated T1 maps by either averaging the T1 maps

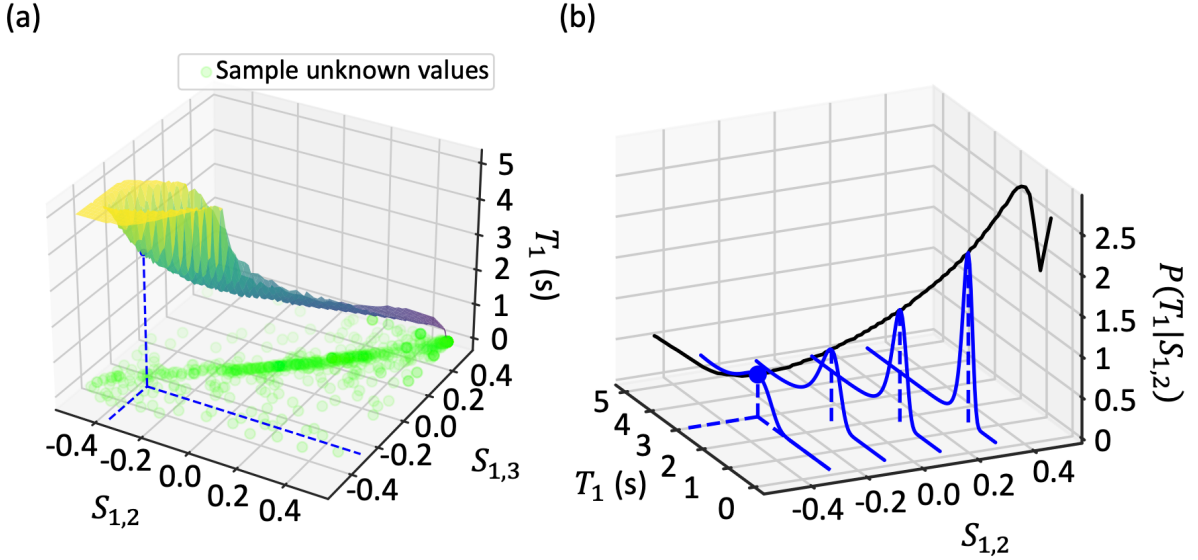


Fig. 2. To extend T1 mapping from MP2RAGE with a single T1-weighted image to MP3RAGE with multiple T1-weighted images (a) and allow for uncertainty estimation, we aim to find the posterior distribution of T1 given $S_{1,2}$ and $S_{1,3}$ (b). Using a Monte Carlo simulation to generate the posterior distribution, we can provide statistical measures such as the MAP estimate or standard deviation of T1.

from the multiple T1-weighted images as in Sun et al. [15], least-squares fitting between the two signals as in Hung et al. [18], or performing T1 mapping using only one of the T1-weighted images as in Metere et al. and Caan et al. [13,14]. Here, to generalize MP2RAGE T1 mapping to MP3RAGE and allow for uncertainty estimation, we propose a MAP approach to T1 mapping (Fig. 2). To estimate MAP T1, we perform a Monte Carlo simulation, calculating the values of the gradient echo readouts (GREs) based on the acquisition parameters and the MP2RAGE signal equations [10], adding Gaussian noise based on a noise level estimate, and using these calculated GRE values to find what the corresponding values of the T1-weighted image $S_{1,2}$ and/or $S_{1,3}$ for both MP2RAGE and MP3RAGE.

Noise in complex-valued MRI acquisitions is well-modeled by a Gaussian for the real and imaginary parts [31]. To measure the estimated noise level, we computed the standard deviation of the values in the corpus callosum of all acquired GREs from an example subject. We manually selected an ellipsoidal region of interest in the corpus callosum. We chose the largest

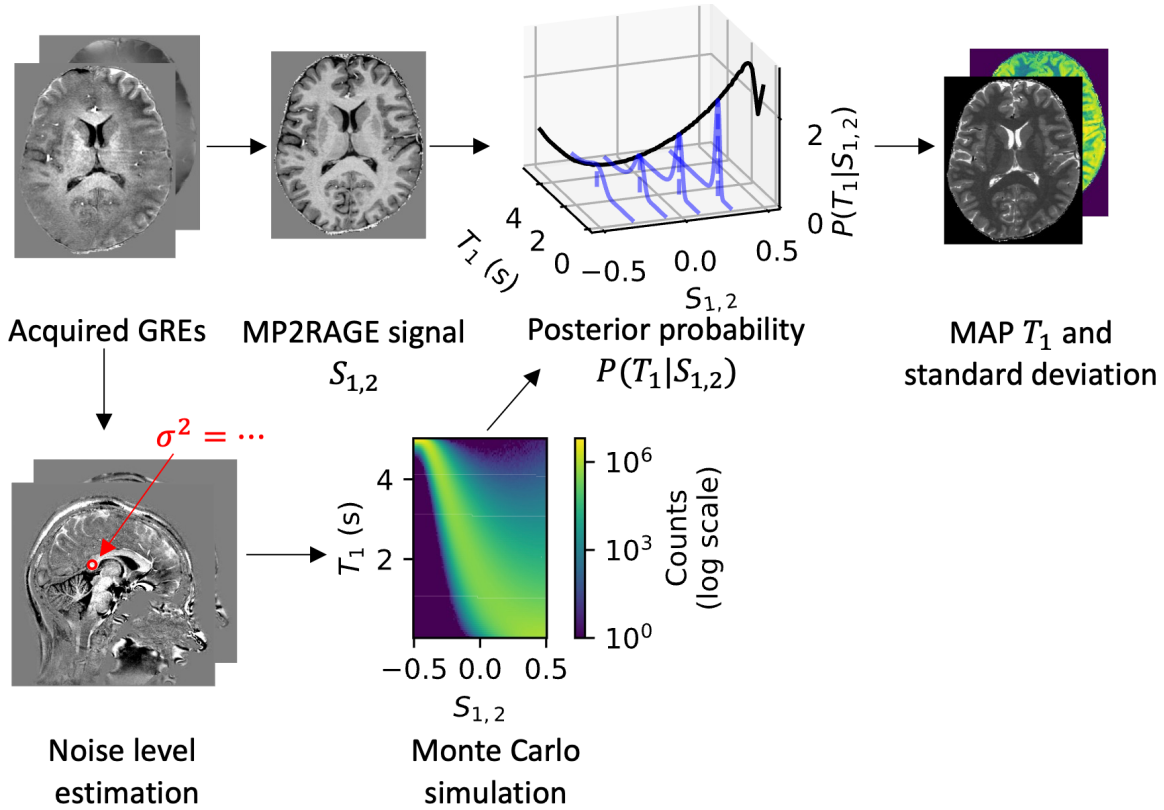


Fig. 3. Generating our MAP T1 estimate from an MP2RAGE signal involves creating a posterior distribution $P(T_1|S_{1,2})$. We measured the noise level in the corpus callosum of the acquired GREs and ran a Monte Carlo simulation to find the values of the MP2RAGE T1-weighted signal $S_{1,2}$ from the GREs with additive Gaussian noise. We normalized the counts generated across all values of T1 for each value of $S_{1,2}$ to form the posterior distribution, from which we calculated the MAP estimate of T1 and the standard deviation of T1.

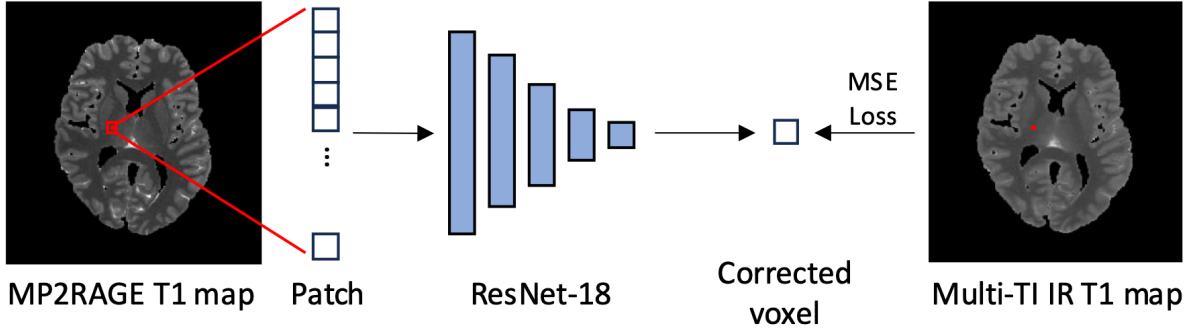


Fig. 4. Calibrating the MP2RAGE T1 map to the multi-TI IR T1 map involves inputting a patch of voxels from the MP2RAGE T1 map into a ResNet-18 model that outputs a single corrected voxel value, which we compare to the multi-TI IR T1 value at the center of the patch using mean square error (MSE) loss.

standard deviation across all real and imaginary parts of the acquired GREs and scaled it to have approximately the same contrast-to-noise ratio for the range of calculated GRE values using the MP2RAGE signal equations. We used the same value of noise in quadrature for the real and imaginary parts of all the GREs for the Monte Carlo simulation. We ran the Monte Carlo simulation for 10 million trials for a range of linearly spaced B1 correction factors ranging from 0 to 2.

From this Monte Carlo simulation, we found the posterior distribution $P(T_1|S_{1,2})$ at a given B1 correction factor by normalizing the counts produced across the range of T1 values for each value of $S_{1,2}$ and B1 correction factor. From this distribution, we can calculate any statistical metric of interest. Here, we calculated the MAP estimate of T1, $T_{1_{MAP}} = \underset{T_1}{\operatorname{argmax}} P(T_1|S_{1,2})$. We calculated the standard deviation of T1 to serve as an uncertainty estimate (Fig. 3). To extend this method to multiple MP2RAGE signals, we can run the Monte Carlo simulation for three or more inversion times and normalize the counts across pairs of T1-weighted images $S_{1,2}, S_{1,3}$, and so on. We can then calculate metrics for the joint distribution $P(T_1|S_{1,2}, S_{1,3})$ using information from all three acquired GREs.

We compared the original point estimate MP2RAGE T1 maps, the MAP MP2RAGE/MP3RAGE T1 maps, and the multi-TI IR T1 maps, all registered to multi-TI IR space. We qualitatively compared the error maps between the methods and calculated the root mean square error (RMSE) for the WM, SGM, and CGM for quantitative comparison. We performed a Bland-Altman-style analysis where we compared the voxelwise error for each method to the multi-TI IR value to describe the bias and variance for each tissue type.

To correct differences between the MAP MP2RAGE T1 maps and multi-TI IR T1 maps, we trained a patch-based ResNet-18 [32]. We used leave-one-out cross-validation across the four subjects, training on two subjects, validating on one subject, and testing on the final subject. The input to the network is a 5×5 patch from an axial slice of the MP2RAGE T1 map, and the

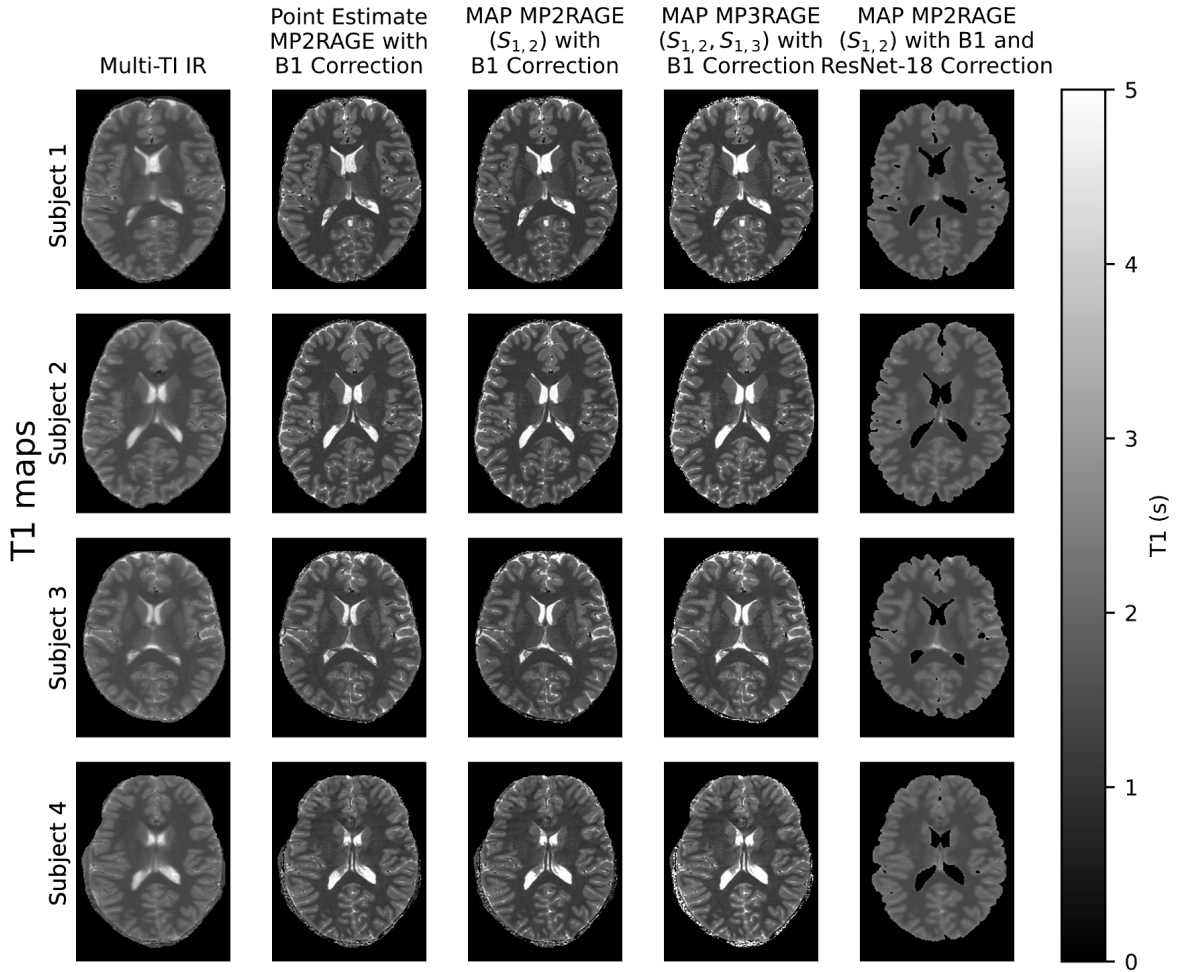


Fig. 5. After performing B1 correction, the MAP MP2RAGE T1 maps appear qualitatively similar to the original point estimate T1 maps, both for MP2RAGE and MP3RAGE. The differences in MP2RAGE T1 maps compared to multi-TI IR T1 maps are not qualitatively apparent from the images alone. Note the ResNet-18 calibration model outputs voxels in the white matter and gray matter only.

output is the multi-TI IR-corrected MP2RAGE T1 value of the center voxel in the patch (Fig. 4). We trained the model using patches whose center voxel lies in the brain tissue (not CSF or background), using mean square error loss between the output voxel value and the multi-TI IR voxel value. We trained using a learning rate of 10^{-5} using batches of 256 patches for 10,000 steps, checking the validation loss every 50 steps and stopping early if the validation loss has not decreased in 1,000 steps. We trained the model both using the MP2RAGE T1 patches alone as well as with the standard deviation as a second channel for the input image, aiming to provide the network with uncertainty information to assist in calibrating the MP2RAGE values.

Next, we tested the sensitivity of our calibration network to the patch size and the noise level estimate. We trained the network on patch sizes of 1×1 , 5×5 , 9×9 , and 13×13 with a constant noise level standard deviation of 0.005. Then, we trained the network on MAP MP2RAGE T1

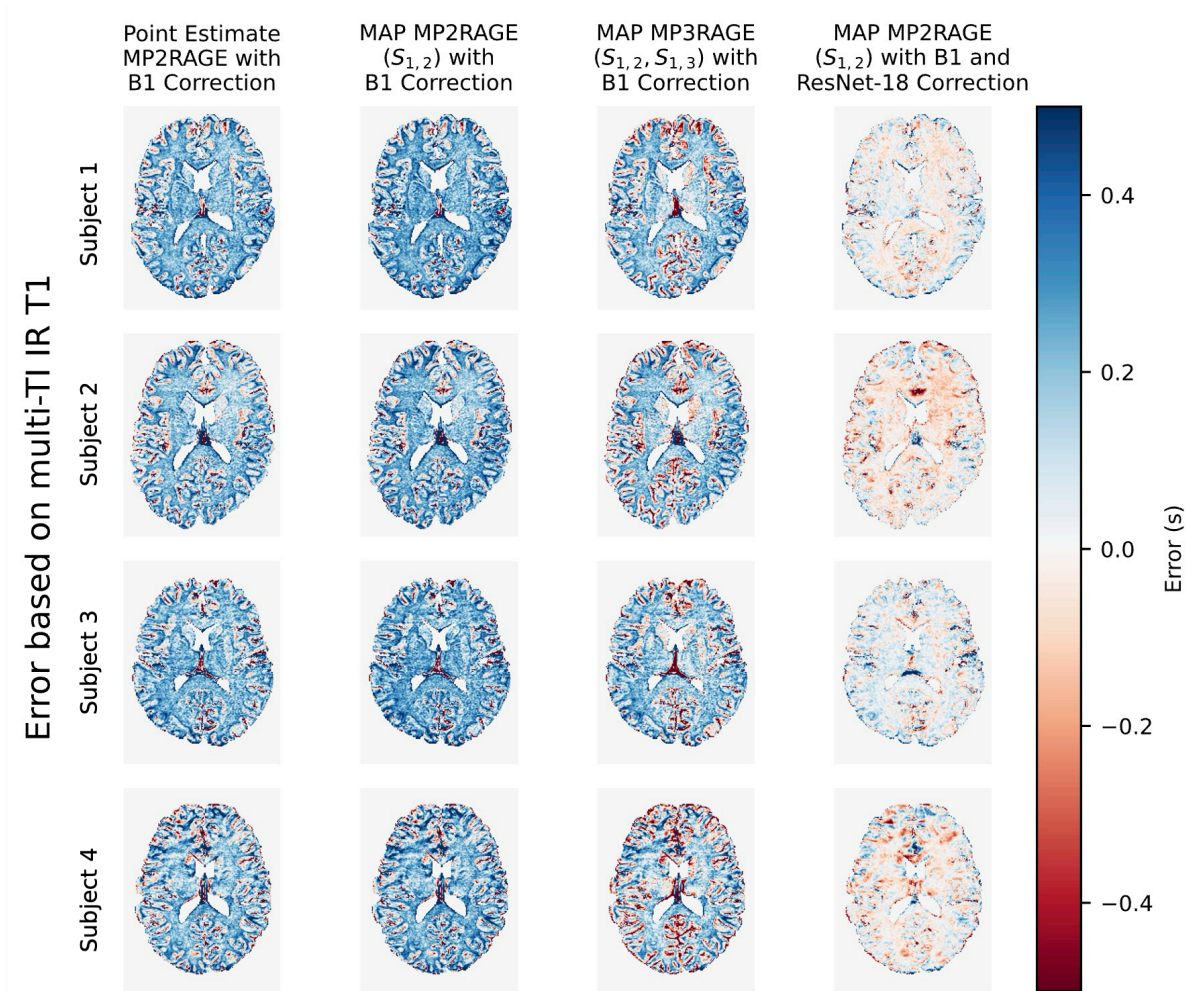


Fig. 6. There is a substantial error between all of the MP2RAGE T1 maps and the multi-T1 IR T1 maps. The patch-based ResNet-18 calibration model reduces this error, though slightly overcorrecting the error in some areas.

maps generated using noise level standard deviations of 0.001, 0.005, 0.01, 0.015, and 0.02 with a constant patch size of 5×5 . For the Monte Carlo simulations in the noise level parameter sweep, we ran 1 million trials. We trained the calibration neural networks for the parameter sweeps the same as above.

To test the significance of the calibration network, we compared the mean RMSE across folds of the MAP MP2RAGE T1 maps with B1 and ResNet-18 correction to the mean RMSE across folds for the MAP MP2RAGE T1 with B1 correction alone. We investigated the performance of the network with the T1 patch alone as well as with the T1 patch with the standard deviation channel. We validate the performance of the network using a paired t -test with a significance level of $\alpha = 0.05$.

Table 1. T1 values across methods and RMSE compared to multi-TI IR T1 values.

| Method | Tissue Type* | Average T1 value (s) | Average RMSE (s) |
|---|--------------|----------------------|------------------|
| Multi-TI IR (with B1 correction) | WM | 1.48 ± 0.03 | -- |
| | SGM | 1.74 ± 0.05 | -- |
| | CGM | 2.05 ± 0.03 | -- |
| MP2RAGE (no B1 correction) | WM | 1.28 ± 0.04 | 0.26 ± 0.02 |
| | SGM | 1.57 ± 0.08 | 0.26 ± 0.03 |
| | CGM | 2.10 ± 0.06 | 0.40 ± 0.03 |
| MP2RAGE (with B1 correction) | WM | 1.22 ± 0.04 | 0.30 ± 0.01 |
| | SGM | 1.55 ± 0.07 | 0.26 ± 0.02 |
| | CGM | 1.96 ± 0.05 | 0.36 ± 0.02 |
| MP2RAGE (B1 + ResNet-18 correction, T1 channel only) | WM | 1.50 ± 0.03 | 0.11 ± 0.02 |
| | SGM | 1.75 ± 0.06 | 0.10 ± 0.02 |
| | CGM | 2.04 ± 0.03 | 0.17 ± 0.03 |
| MP2RAGE (B1 + ResNet-18 correction, T1 and uncertainty channel) | WM | 1.50 ± 0.03 | 0.11 ± 0.02 |
| | SGM | 1.74 ± 0.06 | 0.10 ± 0.02 |
| | CGM | 2.04 ± 0.03 | 0.17 ± 0.03 |

*WM: white matter, SGM: subcortical gray matter, CGM: cortical gray matter

3. Results

The original point estimate MP2RAGE T1 values with B1 correction appear qualitatively similar to the MAP MP2RAGE/MP3RAGE T1 values (Fig. 5). The MAP MP2RAGE and MAP MP3RAGE T1 maps appear similar as well. Though the MP2RAGE and MP3RAGE T1 maps are all comparable, they all have a substantial error compared to the multi-TI IR T1 maps (Fig. 6). The patch-based ResNet-18 calibration model reduces the magnitude of the error for each of the subjects, although it appears to slightly overcorrect in portions of the brain, overestimating T1 in the areas where the MP2RAGE T1 value underestimated compared to multi-TI IR.

The calibration ResNet-18 significantly reduces the RMSE in the WM, SGM and CGM, both using the T1 channel alone as well as using the T1 channel and standard deviation channel (Fig. 7). Table 1 provides the mean T1 value and standard deviation of T1 across subjects for each method, as well as the mean RMSE and standard deviation of RMSE across folds compared to multi-TI IR T1 values. For the patch-based ResNet-18, the addition of the standard deviation as a second channel for the input patches to the network does not substantially change the RMSE compared to the T1 channel alone.

A Bland-Altman-style comparison plotting the error between multi-TI IR T1 values and MP2RAGE values versus multi-TI IR T1 values demonstrates that the B1-corrected MAP MP2RAGE T1 values are not substantially different from the original B1-corrected point estimate MP2RAGE T1 values (Fig. 8). Both methods tend to underestimate T1 compared to

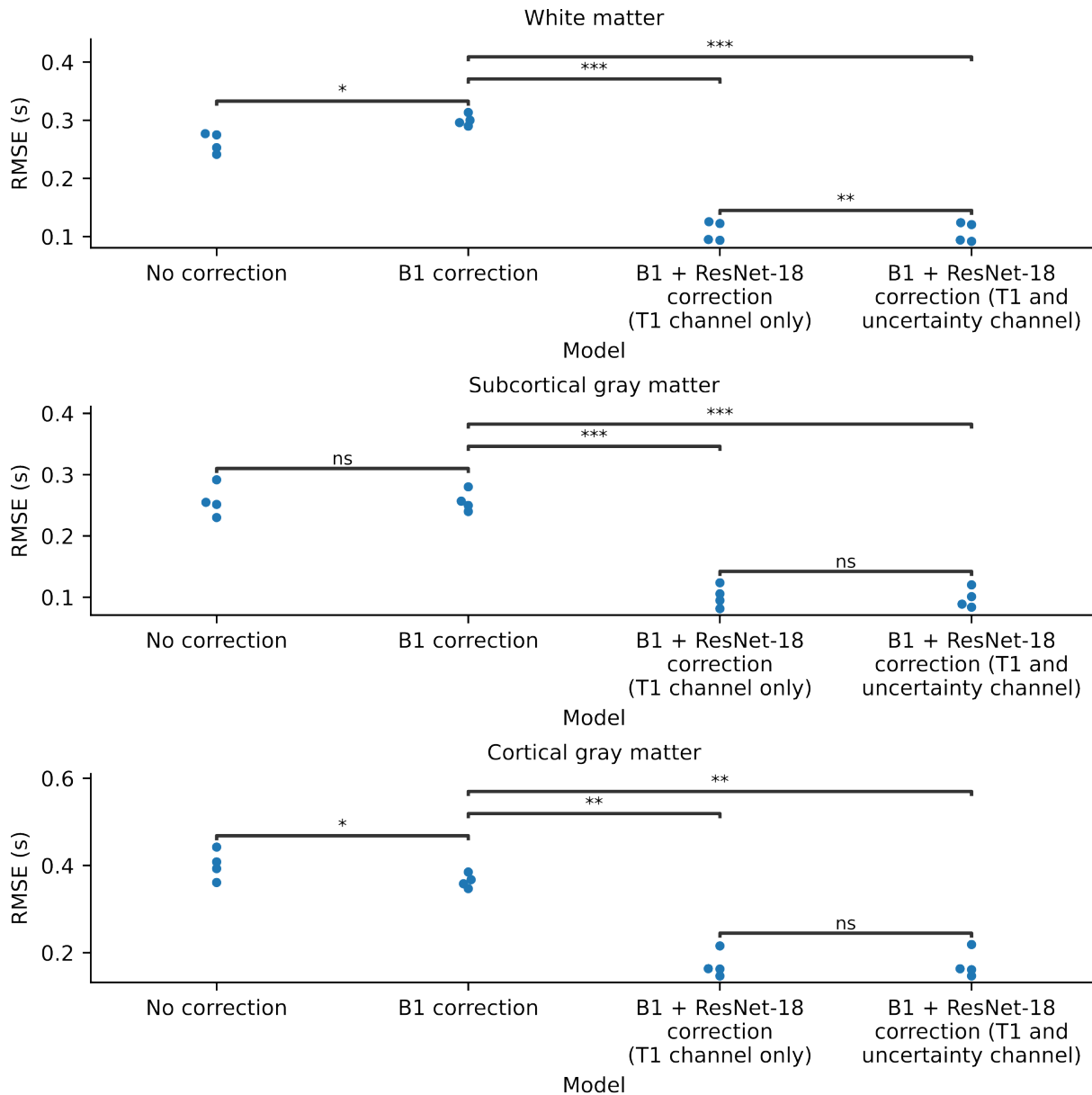


Fig. 7. Using B1 correction alone results in a significant change in RMSE in the white matter and cortical gray matter, but not in the subcortical gray matter. The calibration ResNet-18 model significantly reduces the tissue-dependent bias compared to B1 correction alone in all tissue types. The addition of the uncertainty estimate as a second channel to the network does not substantially change the RMSE across the four folds for all tissue types except white matter. *: $p < 0.05$, **: $p < 0.01$, ***: $p < 0.001$, ns: not significant using a paired t -test.

multi-TI IR. There is a very large variance in the error in both tissue types, with a slightly lower variance in the WM and SGM than in the CGM. The patch-based ResNet-18 calibration network reduces the magnitude of the bias in both tissue types. Additionally, the network reduces the variance of the error in both tissue types.

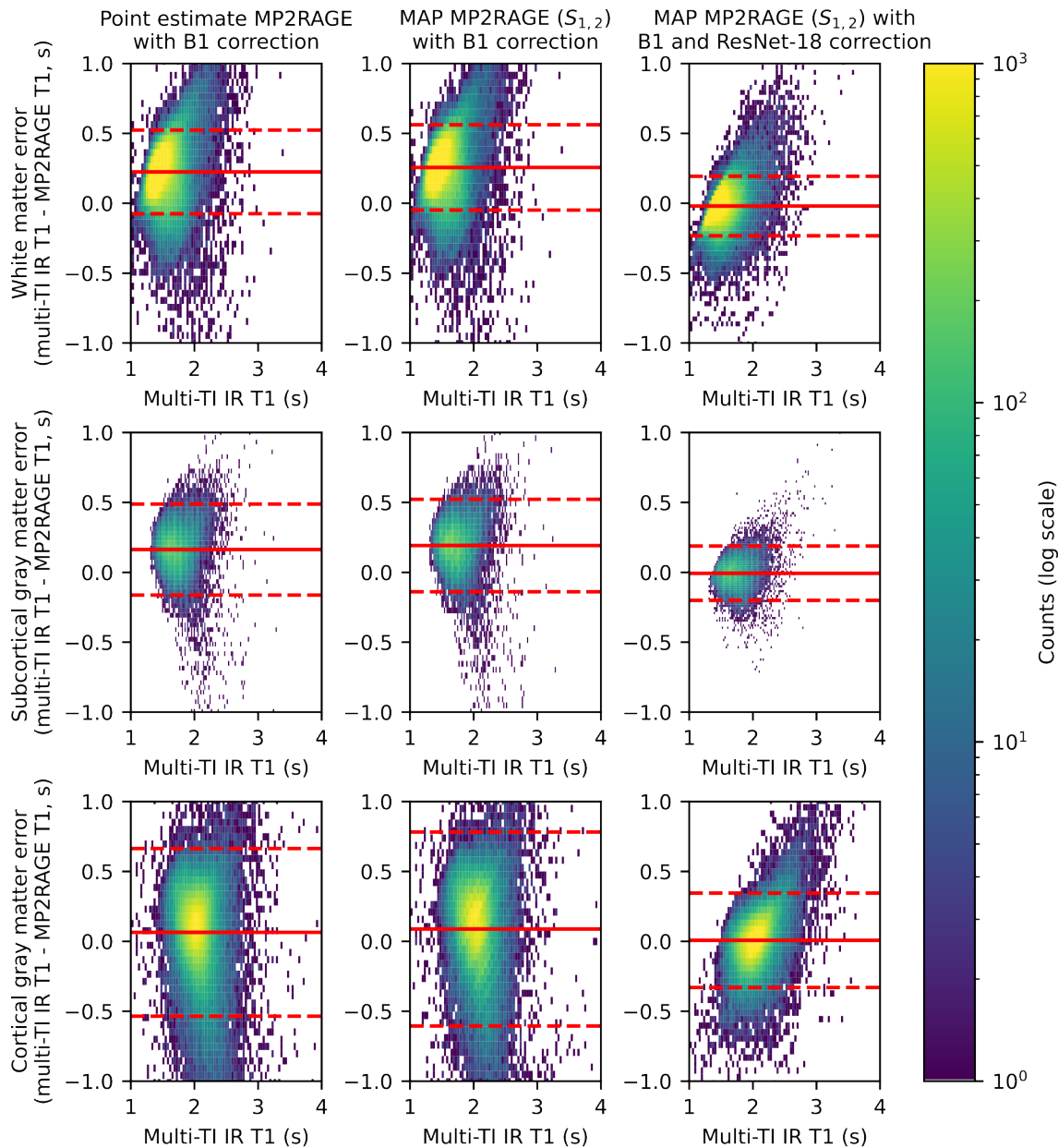


Fig. 8. Bland-Altman-style comparison between the MP2RAGE T1 maps and multi-TI IR T1 maps demonstrates high variance in the error for the original point estimate MP2RAGE and MAP MP2RAGE with B1 correction, as well as a bias in all tissue types. The patch-based ResNet-18 calibration model reduces the bias and moderately reduces the variance, though the cortical gray matter variance remains high after calibration. Solid lines indicate mean error, while dashed lines indicate plus/minus 1.96 times the standard deviation.

The calibration network's performance depends slightly on patch size, with a patch size of 5×5 performing the best (Fig. 9). The RMSE of the MP2RAGE MAP T1 maps depends heavily on the standard deviation of the noise level selected for the Monte Carlo simulation, with higher

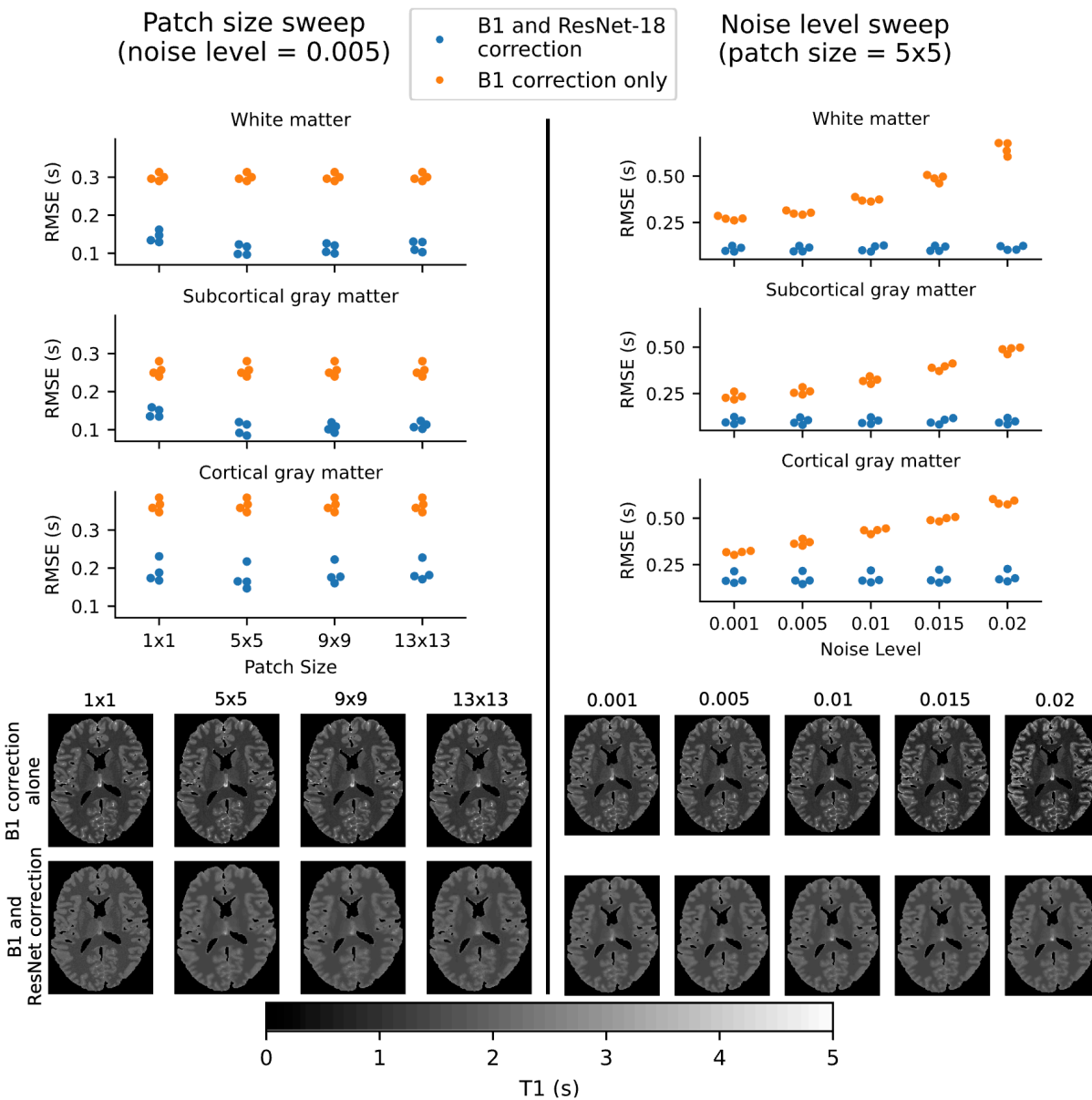


Fig. 9. The ResNet-18 calibration model’s performance depends on the amount of spatial context provided with the patch size, with 5×5 performing slightly better than the other patch sizes. The RMSE produced by MAP MP2RAGE T1 maps increases with higher standard deviations of noise for the Monte Carlo simulation, but the calibration model corrects this error to a relatively constant value across different values of the noise level, albeit with a higher variance in the RMSE.

values of the noise level resulting in higher RMSE. However, the calibration network achieves a similar corrected RMSE across all values of the noise level.

4. Discussion

There are substantial differences between MP2RAGE/MP3RAGE T1 values and multi-TI IR T1 values, but we found that the error between the methods can be significantly reduced with a patch-based neural network trained on limited subjects. The MAP approach allows us to generate any statistical metric of interest, but adding the standard deviation as an uncertainty channel for

the calibration network did not substantially reduce the error. The sensitivity analysis reveals that the calibration network performs best with some spatial context, as a voxelwise correction does not perform as well as patch-based corrections. We found a low noise level works best for the Monte Carlo simulation.

Previous work by Bottomley et al. in 1987 aggregated reported T1 values from over 200 studies and fit the T1 values to a model of the form $T_1 = Av^B$, where v is the Larmor frequency and A and B are tissue-dependent and pathology-dependent constants [33]. Using their model for normal tissue at a Larmor frequency of 300 MHz for 7T, the white matter should fall within 1.12 s to 1.58 s, and gray matter should fall within 1.23 s to 1.73 s. Though they report a wide range of values and only had access to data with a maximum field strength of about 2T due to limitations in data and technology available at the time, our reported T1 values overlap with these intervals nearly 40 years later.

While this study demonstrated the feasibility of calibrating quantitative T1 methods through a patch-based neural network, the use of a neural network for calibrating the T1 values does not explain why there are differences between the methods. Despite the significant reduction in RMSE from our calibration network, there remains a large variance in voxelwise error between multi-TI IR T1 values and MP2RAGE T1 values. Rioux et al. proposed that the difference may be due to the biexponential model for multi-TI IR, while MP2RAGE has limited samples and must use a monoexponential model that cannot account for magnetization transfer effects [21]. However, after our calibration network, the mean differences between quantitative T1 values between the methods are similar in magnitude to differences reported between different quantitative T1 mapping methods at 7T in the literature [8,10,34–36].

5. Conclusion

Here, we demonstrated a method for generating a posterior distribution for MP2RAGE T1 values that can allow for T1 mapping across MP2RAGE and MP3RAGE and generate statistical metrics like the standard deviation of T1. We found a tissue-dependent bias between MP2RAGE/MP3RAGE T1 maps and multi-TI IR T1 maps in both the original point estimate MP2RAGE T1 values as well as in the MAP MP2RAGE/MP3RAGE T1 values. To address the spatially dependent differences between the methods, we demonstrated that a patch-based ResNet-18 trained on registered MP2RAGE and multi-TI IR T1 maps can reduce the error between the two methods by decreasing the magnitude of the bias and reducing the variance of the error. We described differences between these quantitative T1 methods, a neural network can calibrate one method to the other and reduce the error using limited paired training data. This method allows for combining quantitative MRI across multiple acquisitions where the parameters of interest were collected under different acquisitions.

Acknowledgements

This work was supported by NIH grants 1R01EB017230, 5K01EB030039, 5F32NS101788, K01EB032898, and National Cancer Institute R01 CA253923. This work was supported by

Integrated Training in Engineering and Diabetes, grant number T32 DK101003. This work was conducted in part using the resources of the Center for Human Imaging at the Vanderbilt University Institute of Imaging Science (NIH OD award number 1S10OD030389-01) and the Advanced Computing Center for Research and Education at Vanderbilt University, Nashville, TN. The Vanderbilt Institute for Clinical and Translational Research (VICTR) is funded by the National Center for Advancing Translational Sciences (NCATS) Clinical Translational Science Award (CTSA) Program, Award Number 5UL1TR002243-03. The content is solely the responsibility of the authors and does not necessarily represent the official views of the NIH.

Declaration of generative AI and AI-assisted technologies in the writing process

During the preparation of this work the author(s) used GitHub Copilot in order to create code segments based on task descriptions, as well as to debug, edit, and autocomplete code, and ChatGPT to assist in structuring sentences and performing grammatical checks. After using this tool/service, the authors reviewed and edited the content as needed and take full responsibility for the content of the publication.

References

- [1] Weiskopf N, Edwards LJ, Helms G, Mohammadi S, Kirilina E. Quantitative magnetic resonance imaging of brain anatomy and in vivo histology. *Nature Reviews Physics* 2021;3:570–88. <https://doi.org/10.1038/s42254-021-00326-1>.
- [2] Bonnier G, Roche A, Romascano D, Simioni S, Meskaldji DE, Rotzinger D, et al. Multicontrast MRI quantification of focal inflammation and degeneration in multiple sclerosis. *Biomed Res Int* 2015;2015. <https://doi.org/10.1155/2015/569123>.
- [3] Taylor AJ, Salerno M, Dharmakumar R, Jerosch-Herold M. T1 Mapping Basic Techniques and Clinical Applications. *JACC Cardiovasc Imaging* 2016;9. <https://doi.org/10.1016/j.jcmg.2015.11.005>.
- [4] Granziera C, Wuerfel J, Barkhof F, Calabrese M, De Stefano N, Enzinger C, et al. Quantitative magnetic resonance imaging towards clinical application in multiple sclerosis. *Brain* 2021;144:1296–311. <https://doi.org/10.1093/BRAIN/AWAB029>.
- [5] Tsialios P, Thrippleton M, Glatz A, Pernet C. Evaluation of MRI sequences for quantitative T1 brain mapping. *J Phys Conf Ser* 2017;931:012038. <https://doi.org/10.1088/1742-6596/931/1/012038>.
- [6] Gowland P, Mansfield P. Accurate measurement of T1 in vivo in less than 3 seconds using echo-planar imaging. *Magn Reson Med* 1993;30:351–4. <https://doi.org/10.1002/mrm.1910300312>.
- [7] Sanchez Panchuelo RM, Mougín O, Turner R, Francis ST. Quantitative T1 mapping using multi-slice multi-shot inversion recovery EPI. *Neuroimage* 2021;234:117976. <https://doi.org/10.1016/j.neuroimage.2021.117976>.
- [8] Bagnato F, Hametner S, Franco G, Pawate S, Sriram S, Lassmann H, et al. Selective inversion recovery quantitative magnetization transfer brain MRI at 7T: Clinical and post-

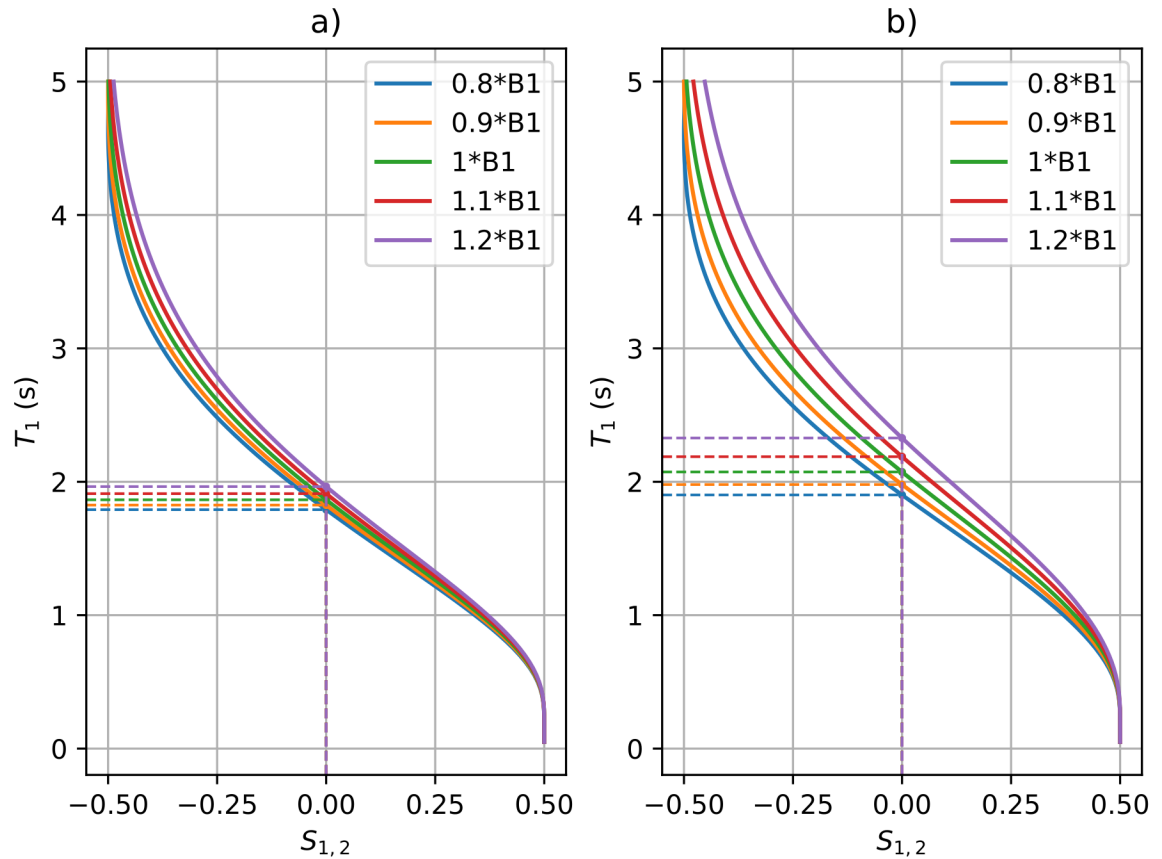
- mortem validation in multiple sclerosis. *J Neuroimaging* 2018;28:380.
<https://doi.org/10.1111/JON.12511>.
- [9] McKeithan LJ, Lyttle BD, Box BA, O’Grady KP, Dortch RD, Conrad BN, et al. 7T quantitative magnetization transfer (qMT) of cortical gray matter in multiple sclerosis correlates with cognitive impairment. *Neuroimage* 2019;203:116190.
<https://doi.org/10.1016/j.neuroimage.2019.116190>.
- [10] Marques JP, Kober T, Krueger G, van der Zwaag W, Van de Moortele PF, Gruetter R. MP2RAGE, a self bias-field corrected sequence for improved segmentation and T1-mapping at high field. *Neuroimage* 2010;49:1271–81.
<https://doi.org/10.1016/J.NEUROIMAGE.2009.10.002>.
- [11] Eggenschwiler F, Kober T, Magill AW, Gruetter R, Marques JP. SA2RAGE: A new sequence for fast B1+-mapping. *Magn Reson Med* 2012;67:1609–19.
<https://doi.org/10.1002/mrm.23145>.
- [12] Voelker MN, Kraff O, Goerke S, Laun FB, Hanspach J, Pine KJ, et al. The traveling heads 2.0: Multicenter reproducibility of quantitative imaging methods at 7 Tesla. *Neuroimage* 2021;232:117910. <https://doi.org/10.1016/J.NEUROIMAGE.2021.117910>.
- [13] Caan MWA, Bazin P, Marques JP, de Hollander G, Dumoulin SO, van der Zwaag W. MP2RAGEME: T1, T2*, and QSM mapping in one sequence at 7 tesla. *Hum Brain Mapp* 2019;40:1786–98. <https://doi.org/10.1002/hbm.24490>.
- [14] Metere R, Kober T, Möller HE, Schäfer A. Simultaneous Quantitative MRI Mapping of T1, T2* and Magnetic Susceptibility with Multi-Echo MP2RAGE. *PLoS One* 2017;12:e0169265. <https://doi.org/10.1371/journal.pone.0169265>.
- [15] Sun H, Cleary JO, Glarin R, Kolbe SC, Ordidge RJ, Moffat BA, et al. Extracting more for less: multi-echo MP2RAGE for simultaneous T1-weighted imaging, T1 mapping, R2* mapping, SWI, and QSM from a single acquisition. *Magn Reson Med* 2020;83:1178–91.
<https://doi.org/10.1002/MRM.27975>.
- [16] Kecskemeti S, Samsonov A, Hurley SA, Dean DC, Field A, Alexander AL. MPnRAGE: A technique to simultaneously acquire hundreds of differently contrasted MPRAGE images with applications to quantitative T1 mapping. *Magn Reson Med* 2016;75:1040.
<https://doi.org/10.1002/MRM.25674>.
- [17] Olsson H, Andersen M, Kadhim M, Helms G. MP3RAGE: Simultaneous mapping of T1 and B1+ in human brain at 7T. *Magn Reson Med* 2022;87:2637–49.
<https://doi.org/10.1002/MRM.29151>.
- [18] Hung W-F, Chen P-T, Chuang T-C, Chang H-C, Wu M-T. High resolution volumetric T1 mapping using a novel MP3RAGE method. *International Society of Magnetic Resonance in Medicine*, 2013.
- [19] Gochberg DF, Gore JC. Quantitative magnetization transfer imaging via selective inversion recovery with short repetition times. *Magn Reson Med* 2007;57:437–41.
<https://doi.org/10.1002/mrm.21143>.

- [20] Cronin MJ, Xu J, Bagnato F, Gochberg DF, Gore JC, Dortch RD. Rapid Whole-Brain Quantitative Magnetization Transfer Imaging using 3D Selective Inversion Recovery Sequences. *Magn Reson Imaging* 2020;68:66. <https://doi.org/10.1016/J.MRI.2020.01.014>.
- [21] Rioux JA, Levesque IR, Rutt BK. Biexponential longitudinal relaxation in white matter: Characterization and impact on T1 mapping with IR-FSE and MP2RAGE. *Magn Reson Med* 2016;75:2265–77. <https://doi.org/10.1002/mrm.25729>.
- [22] Yu X, Yang Q, Zhou Y, Cai LY, Gao R, Lee HH, et al. UNesT: Local spatial representation learning with hierarchical transformer for efficient medical segmentation. *Med Image Anal* 2023;90:102939. <https://doi.org/10.1016/J.MEDIA.2023.102939>.
- [23] Asman AJ, Dagley AS, Landman BA. Statistical label fusion with hierarchical performance models. In: Ourselin S, Styner MA, editors., 2014, p. 90341E. <https://doi.org/10.1117/12.2043182>.
- [24] Hoopes A, Mora JS, Dalca A V., Fischl B, Hoffmann M. SynthStrip: skull-stripping for any brain image. *Neuroimage* 2022;260:119474. <https://doi.org/10.1016/J.NEUROIMAGE.2022.119474>.
- [25] Avants BB, Tustison NJ, Song G, Cook PA, Klein A, Gee JC. A Reproducible Evaluation of ANTs Similarity Metric Performance in Brain Image Registration. *Neuroimage* 2011;54:2033. <https://doi.org/10.1016/J.NEUROIMAGE.2010.09.025>.
- [26] O'Brien KR, Kober T, Hagmann P, Maeder P, Marques J, Lazeyras F, et al. Robust T1-Weighted Structural Brain Imaging and Morphometry at 7T Using MP2RAGE. *PLoS One* 2014;9:e99676. <https://doi.org/10.1371/journal.pone.0099676>.
- [27] Dortch RD, Moore J, Li K, Jankiewicz M, Gochberg DF, Hirtle JA, et al. Quantitative magnetization transfer imaging of human brain at 7 T. *Neuroimage* 2013;64:640–9. <https://doi.org/10.1016/j.neuroimage.2012.08.047>.
- [28] Haast RAM, Ivanov D, Uludağ K. The impact of B1+ correction on MP2RAGE cortical T1 and apparent cortical thickness at 7T. *Hum Brain Mapp* 2018;39:2412–25. <https://doi.org/10.1002/hbm.24011>.
- [29] Marques JP, Gruetter R. New Developments and Applications of the MP2RAGE Sequence - Focusing the Contrast and High Spatial Resolution R1 Mapping. *PLoS One* 2013;8:69294. <https://doi.org/10.1371/JOURNAL.PONE.0069294>.
- [30] Yarnykh VL. Actual flip-angle imaging in the pulsed steady state: A method for rapid three-dimensional mapping of the transmitted radiofrequency field. *Magn Reson Med* 2007;57:192–200. <https://doi.org/10.1002/mrm.21120>.
- [31] Gudbjartsson H, Patz S. The Rician Distribution of Noisy MRI Data. *Magn Reson Med* 1995;34:910. <https://doi.org/10.1002/MRM.1910340618>.
- [32] He K, Zhang X, Ren S, Sun J. Deep Residual Learning for Image Recognition 2015.
- [33] Bottomley PA, Hardy CJ, Argersinger RE, Allen-Moore G. A review of 1H nuclear magnetic resonance relaxation in pathology: Are T1 and T2 diagnostic? *Med Phys* 1987;14:1–37. <https://doi.org/10.1118/1.596111>.

- [34] Rooney WD, Johnson G, Li X, Cohen ER, Kim S, Ugurbil K, et al. Magnetic field and tissue dependencies of human brain longitudinal $^1\text{H}_2\text{O}$ relaxation in vivo. *Magn Reson Med* 2007;57:308–18. <https://doi.org/10.1002/mrm.21122>.
- [35] Wright PJ, Mouglin OE, Totman JJ, Peters AM, Brookes MJ, Coxon R, et al. Water proton T₁ measurements in brain tissue at 7, 3, and 1.5T using IR-EPI, IR-TSE, and MPRAGE: results and optimization. *Magnetic Resonance Materials in Physics, Biology and Medicine* 2008;21:121–30. <https://doi.org/10.1007/s10334-008-0104-8>.
- [36] Bluestein KT, Pitt D, Knopp M V., Schmalbrock P. T₁ and proton density at 7 T in patients with multiple sclerosis: an initial study. *Magn Reson Imaging* 2012;30:19–25. <https://doi.org/10.1016/j.mri.2011.07.018>.

Supplementary Materials

Quantitative T1 mapping is sensitive to acquisition parameters and the B1 correction factor (Supplementary Fig. 1).



Supplementary Fig. 1. MP2RAGE T1 values are sensitive to the values of the acquisition parameters, as well as the B1 correction factor. Acquisition parameters are $MP2RAGE_{TR} = 8.25$ s, $TR = 6$ ms, $TI_1 = 1010$ ms, $TI_2 = 3310$ ms, with 225 excitation pulses, flip angles of 4 degrees, and an inversion pulse efficiency of 0.84 for a) as in this study, and $MP2RAGE_{TR} = 8.5$ s, $TR = 6.9$ ms, $TI_1 = 1000$ ms, $TI_2 = 3000$ ms, with 252 excitation pulses, flip angles of 5° , and an inversion pulse efficiency of 0.84 for b) as in a previous study by Choi et al. [1].

References

- [1] Choi S, Spini M, Hua J, Harrison DM. Blood-brain barrier breakdown in non-enhancing multiple sclerosis lesions detected by 7-Tesla MP2RAGE $\Delta T1$ mapping. PLoS One 2021;16:e0249973. <https://doi.org/10.1371/journal.pone.0249973>.